Non-invasive Respiration Rate Monitoring Using a Single COTS TX-RX Pair

Ossi Kaltiokallio, Hüseyin Yiğitler and Riku Jäntti
Dept. of Communications and Networking,
Aalto University
Espoo, Finland
Email: {name.surname}@aalto.fi

Neal Patwari
Dept. of Electrical and Computer Engineering,
University of Utah
Salt Lake City, Utah, USA
Email: npatwari@ece.utah.edu

***Abstract*—Respiratory rate is an important vital sign that can indicate progression of illness but to also predict rapid decline in health. For the purpose, non-contact monitoring systems are becoming more popular due to the self-evident increase in patient comfort. As a cost effective solution for non-invasive breathing monitoring, utilizing the received signal strength measurements of inexpensive transceivers has been proposed. However, the applicability of the available solutions is limited since they rely on numerous sensors. In this work, considerable improvement is made, and a respiratory rate monitoring system based on a single commercial off-the-shelf transmitter-receiver pair is presented. Methods that enable estimation and enhance the accuracy are presented and their effects are evaluated. Moreover, it is empirically demonstrated that the performance of the system is comparable to the accuracy of a high-end device for 3-4 orders of magnitude less price; achieving mean absolute error of 0.12 breaths per minute in the most realistic scenario of the experiments.**

***Index Terms*—received signal strength, COTS transceivers, wireless sensor networks, respiratory rate monitoring**

I. Introduction

Wireless networks are ubiquitous nowadays. Wherever we are, we interact with radio signals as they propagate from transmitter (TX) to receiver (RX) [1, pp. 47-67]. As a consequence, the channel properties change due to temporal fading [2], providing information about our presence and movements. To exploit this opportunity, dense wireless sensor network (WSN) deployments have been recently utilized for example to perform device-free localization [3] and non-contact respiratory rate monitoring [4]; a research topic we address in this paper. These networks use the received signal strength (RSS) measurements of low-cost transceivers for extracting information about people, rendering new sensing possibilities. Most notably, it is not required that people co-operate with the system allowing one to gain situational awareness of the environment non-invasively.

Respiratory rate is an important vital sign and it can be used to monitor progression of illness but to also predict events that need immediate clinical attention such as cardiac arrest [5]. Traditionally, respiratory rate monitoring relies on technologies built upon a sensor that makes a physical contact with the person's body. However, such systems usually are not suitable for long-term monitoring since mobility and comfort of the patient are restricted. To address this problem, non-contact systems have been developed to improve patient comfort and to improve accuracy for medical applications [5]. These systems also enable new application scenarios such as determining the presence of a living entity in a region of interest for security purposes, and vital sign data collection as part of a larger system such as ambient assisted living and elderly care. However, augmenting these systems with respiratory rate monitoring capability depends on the cost and complexity of the setup. For this purpose, an attractive solution is to utilize inexpensive and commercial off-the-shelf (COTS) transceivers to estimate respiration rate using the RSS measurements.

In the context of non-contact breathing rate monitoring, utilizing the RSS measurements of low-cost COTS transceivers has already been investigated by Patwari *et. al* [4], [6]. However, these works make use of numerous transceivers which limit the applicability of the system due to the complex deployment requirements and data collection management needs. In this work, we address these problems by introducing a non-contact breathing rate monitoring system which is composed of two low-cost COTS transceivers; one being the TX and the other being the RX. The proposed system does not require a sophisticated sensing technology, measurement equipment or complex system setup. In addition, the system can be battery powered enabling comprehensive application opportunities and use-case scenarios.

The work in this paper addresses two major problems that are faced when conducting breathing monitoring using RSS measurements of a single TX-RX pair. First of all, exhaling and inhaling causes very small changes in the propagation channel and therefore, the dB change in RSS is relatively small and it is possible that the breathing signal is not observable in the RSS measurements. For example in Fig. 1, breathing is observable at 2.46 GHz whereas at 2.415 GHz it is not. This problem can be addressed by increasing the signal-to-noise ratio (SNR) and utilizing frequency diversity to enrich the information content of noisy RSS measurements. The second problem to be addressed is, other movements of the person (a posture change at $t \approx 517$ s in Fig. 1), which we refer to as *motion interference*, dominate the frequency content of the RSS measurement. Thus, to enable accurate breathing monitoring in the long-run, time instances of motion

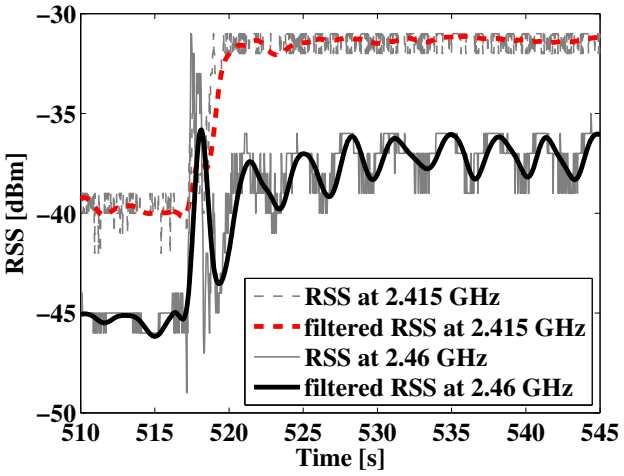

Fig. 1: Measured and filtered RSS of a low-cost TX-RX pair under the influence of a breathing person

interference need to be identified so that breathing monitoring can be disabled during these time intervals.

The proposed breathing monitoring system makes the following contributions:

- Methods to increase the SNR of low resolution RSS measurements are presented. The SNR is increased by: oversampling and filtering, channel diversity, low-jitter periodic communication and directional antennas.
- It is empirically demonstrated that breathing can be accurately estimated using the RSS measurements of a single IEEE 802.15.4 compliant TX-RX pair, significantly improving the existing solutions [4], [6].
- Statistical RSS models are introduced and a hidden Markov model (HMM) is developed to identify motion interference, i.e., time instances when breathing estimation is not possible. The presented RSS models are general characterizations of the channel so that an initial training period is not required by the system.
- Decimation is used to decrease the computational demands of breathing estimation in order to allow embedded realizations of the proposed solution on constraint devices.

Despite the simplicity of the proposed methods, it is demonstrated that the system can achieve accuracy that is comparable to the performance of a high-end device for $3-4$ orders of magnitude less price.

The rest of the paper is organized as follows. Related work is discussed in Section II. Section III introduces the individual components of the breathing monitoring system. Section IV describes the experimental setup used to validate the performance and Section V presents the results. Conclusion are drawn in Section VI.

II. Related Work

Respiratory rate is an important vital sign and it can be used to monitor progression of illness [5] but to also predict events that need immediate clinical attention such as cardiac arrest [7]. In general, breathing monitoring devices can be classified to being either contact or non-contact based. In contact based methods, an instrument is attached to the subject's body to measure for example respiratory airflow, chest/abdominal movement, CO_2 concentration or blood oxygen saturation [5]. On the other hand, non-contact based methods do not make physical contact to the subject's body providing clear advantages such as improved patient comfort and decreased distress [8].

As a potential candidate, RF technologies are finding their way into non-contact respiratory rate monitoring and common approaches include Doppler radar [9] and ultra-wideband [10] based technologies. These systems provide more detailed information about the propagation channel than the RSS measurements. In fact, it has been demonstrated that it is even possible to monitor the heart rate of person using ultra-wideband [11] and Doppler radar [12]. As a drawback, these systems rely on sophisticated and expensive hardware making them impractical in many applications. As an example, the Kai Medical 'Continuous' respiratory rate monitor [13], although not yet FDA approved, is based on Doppler radar and said to be priced at $2000.

As an inexpensive alternative, one can use commercial off-the-shelf narrowband transceivers for estimating the respiration rate of a person. RSS-based breathing monitoring was introduced and experimentally validated in [4]. Moreover, a WSN capable of monitoring and locating a breathing inhabitant in a residential apartment was demonstrated in [6]. However, these systems use numerous transceivers to leverage spatial diversity of the measurements which limits the applicability of the system due to the high complexity. In this work, we address this problem by introducing a breathing monitoring system which is composed of a single COTS TX-RX pair.

Non-invasive vital sign monitoring can create new opportunities not only for improving patient monitoring in hospitals but also in home healthcare applications for example to diagnose and monitor obstructive sleep apnea and sudden infant death syndrome [14]. Other opportunities include: enhancing the life quality of elderly in ambient assisted living applications, to add context-awareness in smart homes, and in search and rescue for earthquake and fire victims.

III. Methodology

A. Breathing Monitoring System

In order to accurately estimate the respiration rate of a person, a breathing monitoring system depicted in Fig. 2 is proposed. First, *Pre-filtering* is applied to increase the SNR of noisy RSS measurements $\boldsymbol{r}(n)$ and down-sampled by a decimation factor M to decrease the computational requirements of the system. Second, *Mean Removal* is applied to the down-sampled signal $\boldsymbol{y}(k)$ because of the used spectral estimation technique and to make the system environment independent so that training is not required. Third, a *Motion Interference Detector* monitors the mean removed RSS measurements,

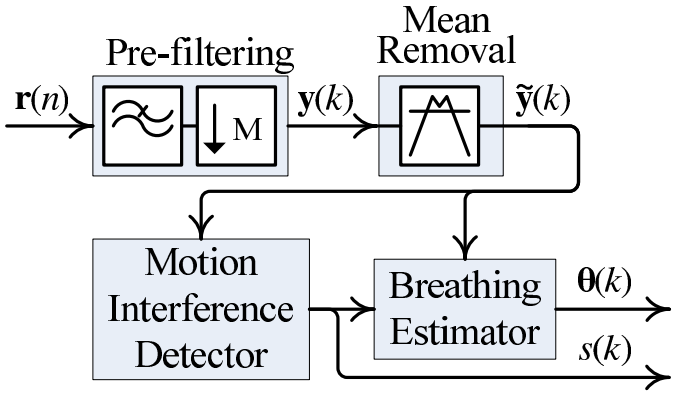

Fig. 2: Overview and components of the breathing monitoring system

denoted by $\tilde{\boldsymbol{y}}(k)$, and the state of the system to enable breathing estimation only when the process is stationary.

The breathing monitoring system has three mutually exclusive states: *no breathing person present* (S_0), *no motion interference* (S_1), and *motion interference* (S_2). To identify whether a breathing person is present, the amplitude estimate in Eq. (12) can be used as suggested in [4]. However, this task is not within the scope of this work and therefore, state S_0 is not considered in remainder of the paper. Furthermore, it is assumed that the current state of the system depends only on the previous state so that the system can be represented by a two-state Markov chain.

B. Pre-filtering

The amplitude of the breathing signal is low and therefore, the quantization error of low resolution radio peripherals can hide the breathing-induced signal. One can increase the SNR of the RSS measurements $\boldsymbol{r}(n)$ by using a higher resolution A/D converter or by over-sampling [15, pp. 182-183]. We adopt the latter option and pre-filter $\boldsymbol{r}(n)$ to increase the SNR and decimate to decrease the computational requirements of breathing estimation. Consequently, the designed pre-filter is a finite impulse response (FIR) decimator.

Considering that breathing frequency f is near 0.23 Hz for adults [16], whereas for newborns f is near 0.62 Hz [17], the filter is designed to have a passband frequency of $f_{min} = 0.1$ Hz and a stopband frequency of $f_{max} = 1$ Hz. The passband ripple of the designed filter is 0.05 dB and the filter has 40 dB attenuation at frequencies higher than 1 Hz. The filter downsamples the measurements by a decimation factor M, thus the sampling frequency at the output is f_s/M, where f_s is the original sampling frequency. We denote the filtered RSS measurements as $\boldsymbol{y}(k)$.

C. Mean Removal

The mean removal subsystem, which essentially is a high-pass filter, provides zero-mean measurements for other components of the system. In [6], the use of a windowed average instead of a 7$^{\text{th}}$ order Chebychev high-pass filter [4] was found superior for the purpose of breathing estimation, i.e.,

$$\boldsymbol{\mu} = \frac{1}{L}\sum_{i=0}^{L-1} \boldsymbol{y}(k-i), \tag{1}$$

where L is the length of the window. Thus, the output of the mean removal subsystem is $\tilde{\boldsymbol{y}}(k) = \boldsymbol{y}(k) - \boldsymbol{\mu}$.

Window length L must be determined according to the system requirements. Small values of L can suppress the spectral components of the breathing-induced signal. On the other hand, selecting L too large can allow frequencies much lower than the minimum breathing rate to remain in $\tilde{\boldsymbol{y}}(k)$. In this paper, we set $L = f_s/M$ so that mean removal acts as a high pass FIR filter with a 3 dB cut-off frequency at approximately 0.2 Hz for $f_s = 31.25$ Hz and $M = 10$.

D. Measurement Model

The pre-filtered and mean removed RSS measurement in dB at time k on frequency channel c containing an additional signal can be written as

$$\tilde{y}_c(k) = g_c(k) + \epsilon_c(k), \tag{2}$$

where $g_c(k)$ is an unknown signal, and $\epsilon_c(k)$ is wide sense stationary noise with zero-mean and variance σ^2. When a breathing person is present, it can be assumed that $g_c(k)$ is sinusoidal [4],

$$g_c(k) = A_c \cos(2\pi f T_s k + \phi_c), \tag{3}$$

where A_c, ϕ_c, and f are the amplitude, phase and frequency in respective order and T_s is the sampling period.

The considered transceivers enable communication on multiples of frequency channels. Thus, the RSS measurement in Eq. (2) can be extended to a measurement vector

$$\tilde{\boldsymbol{y}}(k) = \begin{bmatrix} \tilde{y}_1(k) & \tilde{y}_2(k) & \cdots & \tilde{y}_C(k) \end{bmatrix}^T, \tag{4}$$

where C is the number of used frequency channels. Since the periodic component is generated by the breathing person, we assume that the frequency of the breathing-induced signal on the different channels is the same, whereas the amplitude and phase are expected to be channel dependent. Further, the measurement noise contaminating each channel is assumed to be independent. Consequently, the measurement model of the studied system is given by

$$\tilde{\boldsymbol{y}}(k) = \boldsymbol{g}(k) + \boldsymbol{\epsilon}(k), \tag{5}$$

where $\boldsymbol{\epsilon}(k) \sim \mathcal{N}(\boldsymbol{0}, \boldsymbol{\Sigma})$ is zero-mean multivariate Gaussian, having independent components with equal variances, $\boldsymbol{\Sigma} = \sigma^2 \boldsymbol{I}$.

E. Motion Interference Detector

It has already been shown that the RSS experiences time intervals of considerable fading caused by the movements of people, whereas most of the time the RSS remains nearly constant [18]. This fading / non-fading time varying process can be modeled as a two-state Markov chain [19]. However, the states of our system are not directly observable and

therefore, we represent the system using a hidden Markov model (HMM). In order to make the decision of enabling or disabling breathing estimation, the state of the system is estimated through an observable measure, the RSS, which is a probabilistic function of the unobservable state.

The HMM can be used to calculate the probability of an observation $x(k)$ given the state transition probabilities P, the conditional densities of the observations $p_{x|s}$, and the initial state probability γ using the *forward procedure* [20, pp. 109-114]

$$p_x(x(k)|P, p_{x|s}, \gamma) = \sum_{i=1}^{Q} \alpha_i(k), \tag{6}$$

where α is the forward variable and Q is the number of states ($Q = 2$). The forward variable at time instant k for state s_i can be calculated recursively

$$\alpha_i(k) = \left[\sum_{j=1}^{Q} \alpha_j(k-1) \cdot P_{i|j}\right] p_{x|s}(x(k)|s_i), \tag{7}$$

where $\alpha_i(1) = \gamma_i \cdot p_{x|s}(x(1)|s_i)$. The output of the motion interference detector is the state that has the highest probability at time k and it is used to enable/disable breathing estimation. Parameters of the HMM are given in Table I.

F. Conditional Observation Densities

In order to determine the probability of the observation at time instant k, it is mandatory to consider the distribution of the observations given the state of the system. In this paper, our observation for the HMM is the average of the pre-filtered and mean removed RSS measurements

$$x(k) = \frac{1}{C} \sum_{c=1}^{C} \tilde{y}_c(k). \tag{8}$$

In state S_1, the RSS measurements are dominated by quantization errors and electronic noise. Therefore, $x(k)$ is the sum of independent and identically distributed random variables since the mean is removed and the different frequency channels use the same receiver. Due to the central limit theorem, the density of $x(k)$ is expected to be Gaussian with zero-mean

$$p_{x|s}\left(x(k); 0, \sigma\right) = \frac{1}{\sigma\sqrt{2\pi}} \exp\left(-\frac{x(k)^2}{2\sigma^2}\right). \tag{9}$$

Correspondingly, the RSS measurements during motion interference are expected to follow the distribution describing multipath fading since it dominates the other noise sources. Multipath fading is typically represented by the Rayleigh, Ricean or log-normal distribution, each having their own theoretical justification [2]. We use the log-normal distribution to characterize the observations when in state S_2. Thus, in logarithmic scale, $x(k)$ has the Gaussian density given in Eq. (9).

The empirical and theoretical densities of $x(k)$ in the two states are shown in Fig. 3. Using experimental data (see Section IV for details), the empirical distributions are

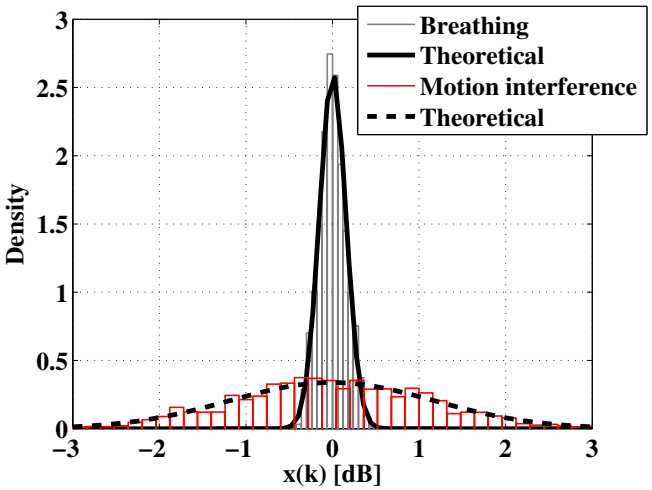

Fig. 3: The empirical and theoretical conditional densities of the observations

generated and tested against the theoretical ones using the Kolmogorov-Smirnov test [21]. From both densities, 1000 samples are drawn and tested with respect to the theoretical distribution with a significance level of 5%. For both tests, the hypothesis that the observations belong to the tested theoretical distribution is accepted. The *p-values* of the statistical tests are 30% and 46% for states S_1 and S_2 in respective order. Parameters of the derived conditional densities are given in Table I.

It is important to note that σ_1 is environment independent and that it represents the RSS changes caused e.g. by electronic noise of the receiver and breathing-induced variations. On the other hand, σ_2 is experiment dependent since e.g. people, the surrounding environment and node distance – all contribute to the temporal fading statistics at the RX. However, since the RSS variations in state S_2 are always much higher than in S_1, it is not necessary to derive exact conditional densities for state S_2 as long as σ_2 is set much larger than σ_1. To this end, even though we conduct experiments using three different hardware configurations, it is not necessary to adjust σ_1 and σ_2 of the distributions for the different hardware to improve the performance of the HMM. In other words, the derived conditional densities are general characterizations of the states and the system does not require a training period before operation.

G. Breathing Estimator

Breathing monitoring aims to use $\tilde{\boldsymbol{y}}(k)$ to estimate $\boldsymbol{g}(k)$ for which the parameters are given as

$$\boldsymbol{\theta} = [\boldsymbol{A}, \boldsymbol{\Phi}, f]^T, \tag{10}$$

where $\boldsymbol{A} = [A_1, \ldots, A_C]$ and $\boldsymbol{\Phi} = [\phi_1, \ldots, \phi_C]$ are the amplitude and phase of the different channels, and f is the common frequency. Given the parameters of $\boldsymbol{g}(k)$, spectral estimation techniques can be utilized to estimate $\boldsymbol{\theta}$ as proposed by Patwari *et al.* [4].

A good estimate of f is the frequency where the power spectral density (PSD) has its maximum

$$\hat{f} = \underset{f_{min} \le f \le f_{max}}{\arg\max} \frac{1}{C} \sum_{c=1}^{C} \left| \sum_{k=1}^{N} \tilde{y}_c(k) e^{-j2\pi f T_s k} \right|^2, \quad (11)$$

where N is the number of samples (window length). After $\hat{f}$ is estimated, it can be used to estimate amplitudes and phases of the different frequency channels using

$$\hat{A}_c = \frac{2}{N} \left| \sum_{k=1}^{N} \tilde{y}_c(k) e^{-j2\pi \hat{f} T_s k} \right|, \quad (12)$$

$$\hat{\phi}_c = \arctan \frac{-\sum_{k=1}^{N} \tilde{y}_c(k) \sin(2\pi \hat{f} T_s k)}{\sum_{k=1}^{N} \tilde{y}_c(k) \cos(2\pi \hat{f} T_s k)}. \quad (13)$$

In general, we are most interested in $\hat{f}$. However, also $\hat{A}_c$ and $\hat{\phi}_c$ contain valuable information about breathing. For example, $\hat{A}_c$ can be used to identify whether a breathing person is present or not [4].

IV. Experiments

A. Measurement Setup

The proposed breathing monitoring system is evaluated using a single antenna pair as illustrated in Fig. 4. One of the antennas is directly connected to the TX node while the other antenna is connected to a directional coupler to enable simultaneous acquisition of the RSS using two different measurement systems. The RX node is connected to one of the outputs of the directional coupler whereas a real-time spectrum analyzer (RSA) is connected to the other. Since the RSA acquires high resolution RSS measurements, it is used as a reference system in experimental evaluation.

We are only interested in the region between the TX-RX pair. Therefore, directional antennas, which provide a 8 dBi gain and 75° horizontal beam width [22], are used in the experiments. As a consequence, the directional antennas increase the quality of the RSS measurements because they diminish the effects of multipath propagation which has severe fading effects in measurement setups that use omni-directional antennas. The used nodes are equipped with Texas Instruments CC2431 IEEE 802.15.4 PHY/MAC compliant transceivers. The transceivers' micro-controller unit runs a communication software and a modified version of the FreeRTOS micro-kernel operating system, both developed by researchers at Aalto University.

The transceivers make use of low-resolution A/D converters, inevitably affecting granularity of the RSS measurements (± 1 dB). To gain deeper understanding of this limitation, the RF signals impinging on the RX antenna are simultaneously measured using a Tektronix's RSA6114A real-time spectrum analyzer, which provides 0.1 dB resolution in amplitude. In DPX mode, the RSA enables spectral representation of multiples of narrow-band pulsating signals with different center frequencies even when the signals are sequential in time [23]. Therefore, the high resolution RSS information of individual narrow-band signals can be calculated using single amplitude trace data of the RSA.

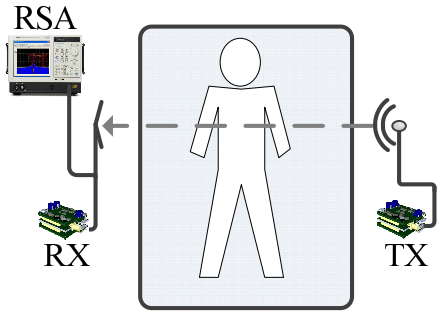

Fig. 4: Experimental setup

In the experiments, the TX node is programmed to transmit packets over each of the 16 frequency channels defined by the IEEE 802.15.4-2006 standard [24] at the 2.4 GHz ISM band. After each transmission, the frequency channel of communication is changed sequentially to cover the complete spectrum. The transmission interval is aligned to 2 ms. Thus, $f_s = 31.25$ Hz for each frequency channel, which is considerably higher than the breathing frequencies of interest.

The RX node is programmed to listen for ongoing transmissions. Upon receptions, the packets are timestamped at the start of frame delimiter with a resolution of $1/32$ microseconds. The packets are stored to a SD memory card of the node for off-line analysis. On average, the time interval between receptions is 2 ms with a standard deviation of 141 microseconds. The proposed measurement setup provides uniformly sampled RSS measurements, a strict requirement of the used spectral estimation technique. In other words, the SNR is not degraded due to irregular sampling.

The RSA is configured to cover the entire band between 2.4 GHz to 2.5 GHz with 500 kHz resolution and to acquire samples for a duration of 128 microseconds in DPX mode of operation. The amplitude trace of the 100 MHz bandwidth is represented using 4001 points. The operation of the RSA is remotely controlled by a portable computer over a GPIB interface. A query is sent to the RSA to measure and return the peak amplitude trace data, on average, once every 337 ms with a standard deviation of 7.3 ms. The acquired trace values together with the time of request information are stored for off-line analysis.

B. Experiments

In order to quantitatively evaluate the performance of the presented system, the TX and RX antennas are placed on opposite sides of a queen-size bed so that the LoS component intersects the chest/abdominal region of the person. This region has been identified the most effective for successful breathing estimation [4]. The bed is located in a typical bedroom which includes a wardrobe, nightstands and other furniture and the antennas are placed 0.20 m above chest height, 2.00 m apart from each other. In the experiments, a person is lying on the bed and following a metronome to set

TABLE I: Experimental parameters

Parameter	Description
$C = 16$	Number of channels
$f_s = 31.25$	Sampling frequency [Hz]
$L = 3$	Window length of mean removal
$M = 10$	Decimation factor
$N = 30$	Estimation window length [s]
$\sigma_1 = 0.152$	Standard deviation in state S_1
$\sigma_2 = 1.18$	Standard deviation in state S_2
$\gamma = [1 \quad 0]$	Initial state probability
$P_{1\|1} = 0.9$	Transition probability from S_1 to S_1
$P_{2\|2} = 0.07$	Transition probability from S_2 to S_2

the pace for breathing. The same setup is used for conducting three different experiments.

The experiments are conducted in a typical apartment building where more than ten Wi-Fi networks are identified to coexist. Even though we do not directly address issues related to interference in this paper, the system is able to cope with coexisting networks. This is because the nodes are equipped with directional antennas, channel diversity is exploited and most importantly, the system is not particularly sensitive to bursty interference and occasional packet drops due to oversampling.

Experiment 1 is designed for studying and validating the accuracy of the breathing monitoring system. In the tests, the person is lying still on their back and breathing at a constant rate for two minutes. The experiment is repeated five times using different respiration rates: 12, 14, 16, 18 and 20 breaths per minute (bpm).

Experiment 2 is designed to evaluate the performance of the HMM. In this experiment the person is asked to change their posture once every minute while breathing at a constant rate of 16 bpm. The sequence of postures is the following: lying on the back, side, stomach and other side. In between the posture changes the person is stationary.

Experiment 3 is used to study adaptivity of the system. It is composed of two tests which combine different aspects of Experiments 1 and 2. In the first test, the person is asked to follow a sequence of breathing rates while staying otherwise stationary. In the second test, the person also changes their posture when the breathing rate is changed.

In the first test of Experiment 3, the person is initially breathing at a rate of 13 bpm. Every half a minute, the breathing rate is increased by half a bpm until the person is breathing at a rate of 18 bpm. After this, the breathing rate is decreased by 0.5 bpm every 30 s until the person is breathing at 15 bpm.

In the second test of Experiment 3, the person is initially breathing at a rate of 12 bpm and every minute, the breathing rate is increased by one bpm until the person is breathing at 19 bpm. After this, the breathing is decreased by one bpm every minute until the person is breathing at 15 bpm. Every time the breathing rate is changed, the person also changes their posture following the sequence described in Experiment 2. The same sequence of postures is repeated throughout the test.

C. Validation Metrics

The components of $\boldsymbol{\theta}$ are estimated only when N samples of $\tilde{\boldsymbol{y}}(k)$ are available. If N is smaller than the duration of the test, $\boldsymbol{\theta}$ is evaluated once every second. For example, considering a single test of Experiment 1 which contains data over a two minute time interval and if N is set to a 30 second time window, then there are in total $K = 91$ estimates of $\boldsymbol{\theta}$ during the same test. During the first 29 seconds of the test, $\boldsymbol{\theta}$ is not evaluated since time index $k < N$.

The breathing rate estimation accuracy of the system is evaluated using mean absolute error after K estimates,

$$\varepsilon_f(K) = 60\frac{1}{K}\sum_{l=1}^{K}|\hat{f}(l) - f(l)|, \tag{14}$$

where $f(l)$ is the rate of the metronome, and $\hat{f}(l)$ is the estimate. The variation of the estimates from the mean is measured with the ratio of estimates inside the confidence interval of 1 bpm,

$$\varepsilon_{\%}(K) = \frac{K - K_o}{K}, \tag{15}$$

where K_o is the number of estimates outside of the confidence interval. We also refer the estimates within the confidence interval as *valid* estimates, and correspondingly, the ones outside of the confidence interval as *invalid* estimates.

Pre-filtering presented in Section III-B is to enhance the performance of RSS-based breathing monitoring when using low-cost wireless devices. Since the RSS measurements of the RSA are already very precise, pre-filtering is not applied to them. Further, a decimation factor of ten is only used with measurements of the node so that approximately the same number of samples is used for estimation with both hardware. The experimental parameters are given in Table I.

V. Results

A. Qualitative Comparison

Inhaling and exhaling causes very small changes in the propagation channel and therefore, the dB change in the RSS measurements is relatively small. Thus, the dynamic range of the receiver and the SNR determine whether the low-amplitude breathing signal is observable in the RSS measurements or not. Analysis of the RSS measurements gathered with the RSA during the tests of Experiment 1 shows that the periodic breathing signal is observable on all 16 frequency channels of every test. For these data, the average RMS amplitude of the breathing signal is 0.155 dB with standard deviation of 0.025 dB. Since the resolution of the node receiver's A/D converter is ± 1 dB, quantization error and electronic noise are likely to dominate the breathing signal. Analyzing the measurements acquired by the receiver node during Experiment 1 exposes that the breathing signal is not resolvable on all channels.

In Fig. 5a, the spectrogram of the RSA measurements in the band containing the first five frequency channels (2.4 – 2.425 GHz) while a person is breathing at a constant rate of 16 bpm is shown. Correspondingly, the RSS measurements

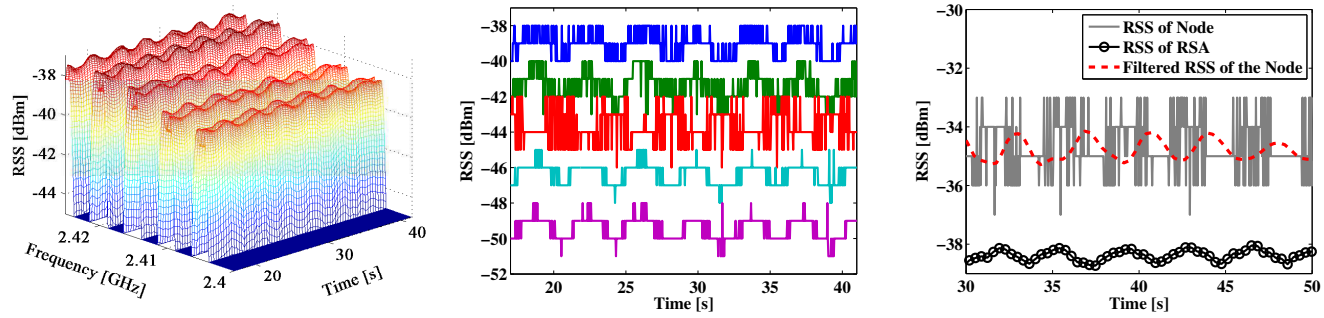

(a) Spectrogram measured with RSA (b) RSS measurements of the node (c) RSS measured with RSA and node

Fig. 5: Qualitative comparison of the measurements. Acquired measurements of the two hardware shown in (a) and (b). The filtered RSS of the node with respect to the RSS measurements of the RSA shown in (c)

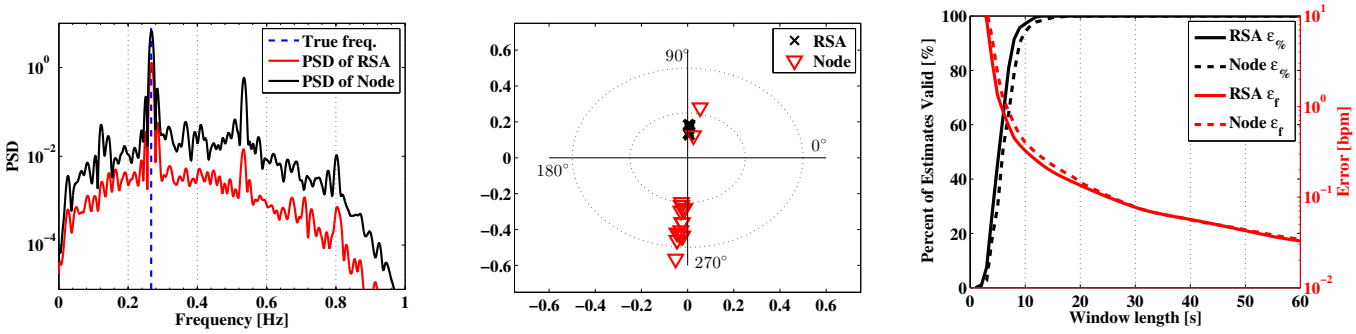

(a) PSDs (b) Polar plot of phase and amplitude (c) Effect of window length

Fig. 6: Example PSDs shown in (a), the individual phase and amplitude estimates in (b), and the effect of window length N to ε_f and $\varepsilon_{\%}$ shown in (c)

of the node on the same five frequency channels is shown in Fig. 5b. For clarity, only the first five channels are illustrated in the figures. Also, the means are shifted in the measurements of Fig. 5b so that data of the different channels do not overlap one another. The high resolution measurements of the spectrum analyzer clearly bring forth the breathing-induced signal as shown in Fig. 5a. Respectively, the RSS measurements of the node also contain a periodic signal but due to the nodes lower quality electronics, the breathing induced signal is not as evident. Applying straightforward yet effective signal processing methods as explained in Section III-B increase the SNR of the RSS measurements considerably as shown in Fig. 5c. Thus, one can acquire high resolution RSS measurements with a low-cost hardware that are comparable to the measurements of a high-end device for $3-4$ orders of magnitude less price.

B. Experiment 1

Example PSDs of $\{\tilde{\boldsymbol{y}}(k)\}_{k=1}^{N}$ of the RSA and node measurements are shown in Fig. 6a. Clearly, the peak amplitude of both PSDs is very close to the true respiration rate. More quantitatively, the breathing rate estimate yields $\varepsilon_f = 0.038$ bpm using the RSA measurements whereas $\varepsilon_f = 0.074$ bpm with the node. Another important observation is the fact that both PSDs show the second and third harmonics of the breathing signal. Consequently, breathing does not cause perfectly sinusoidal variations in the RSS, but rather a periodic waveform which has both odd and even harmonics.

The polar plots of phase and amplitude estimates using $\{\tilde{y}_c(k)\}_{k=1}^{N}$ for each $c = 1, \cdots, 16$ are shown in Fig. 6b. When using the RSA, the estimates correlate highly among each other indicating that a breathing person causes frequency independent changes. Thus, the larger frequency dependent amplitude variations of the node can only result from the node's low-quality electronic components since the measurements are obtained using the same antenna. Because the amplitude estimates of the node vary, it is possible that quantization and electronic noise of the node can hide the breathing-induced RSS changes. Consequently, channel diversity should be used effectively to increase the SNR, to compensate the limitations of the node and to increase the probability that at least one channel captures the breathing-induced changes in the propagation channel.

In Fig. 6c, the effect of window length N to respiration rate monitoring is shown. In the figure, the black lines illustrate $\varepsilon_{\%}$

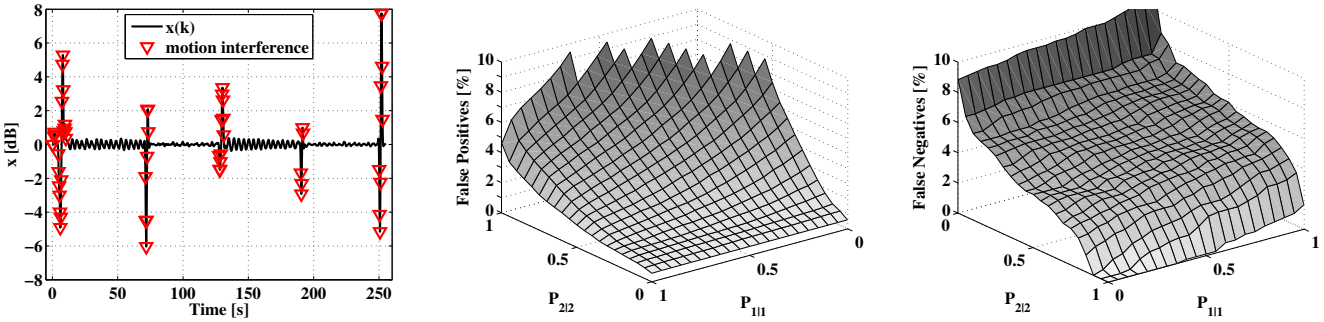

(a) Motion interference instances (b) False positives (c) False negatives

Fig. 7: The performance of the HMM in Experiment 2

TABLE II: Results of Experiment 1 for $K = 91$

	Node		RSA	
f [bpm]	ε_f [bpm]	$\varepsilon_{\%}$ [%]	ε_f [bpm]	$\varepsilon_{\%}$ [%]
12	0.0790	100.0	0.0888	100.0
14	0.0579	100.0	0.0460	100.0
16	0.0743	100.0	0.0746	100.0
18	0.0987	100.0	0.1087	100.0
20	0.0777	100.0	0.0676	100.0

whereas the red lines show ε_f as a function of N. On average, the breathing estimates are more accurate with the RSA than with the node measurements when the window length is below 20 s. However, when the window length is larger, the difference in the estimates between the two systems is negligible. In the following subsections, $N = 94$ [samples] ≈ 30 [seconds], if not otherwise stated.

The estimation accuracy of the proposed system using the measurements of the RSA and the node for tests of Experiment 1 are summarized in Table II. The results reveal that the actual respiration rate does not affect the accuracy of breathing estimation. Further, the results of both measurement systems are very close to each other. Therefore, the processed RSS measurements have a high enough SNR to accurately estimate the breathing rate of a person.

C. Experiment 2

In Fig. 7a, observations $x(k)$ and the motion interference instances triggered by the HMM during Experiment 2 are shown. The HMM correctly detects the posture changes and disables breathing monitoring during these time intervals. The performance of the system in the experiment is $\varepsilon_f = 0.1113$ bpm using the node, whereas $\varepsilon_f = 0.0739$ bpm with the RSA measurements. For both systems, $\varepsilon_{\%} = 100.0\%$.

The detection of motion interference is an essential part of the proposed system and it improves the estimation accuracy significantly. In order to show the effect of the detector, we disable it. In this case, $\varepsilon_f = 0.6970$ bpm using the node, whereas $\varepsilon_f = 0.5889$ bpm with the RSA measurements. These estimates are heavily skewed and the maximum errors are $\max(\varepsilon_f) = 5.5$ bpm with the node and $\max(\varepsilon_f) = 10.0$ bpm using the RSA measurements. In corresponding order, the percentage of valid estimates is $\varepsilon_{\%} = 75.0\%$ and $\varepsilon_{\%} = 93.1\%$. Therefore, to enable accurate breathing estimation in practical applications, identifying motion interference is mandatory.

For practical purposes, it is important to investigate how sensitive the HMM is against the changes in state transition probability matrix P. We evaluate the effect of transition probabilities with the number of *false positive* and *false negative* state transitions. A false positive occurs when the HMM indicates that there is motion interference even though the person is stationary. Correspondingly, a false negative occurs when the person moves but it is not detected. False positives are shown in Fig. 7b and false negatives in Fig. 7c as functions of $P_{1|1}$ and $P_{2|2}$. In general, the number of false positives decreases as $P_{1|1}$ increases and $P_{2|2}$ decreases. However, the number of false negatives increases at the same time. Therefore, the state transition probabilities must be set depending on the performance requirements of the HMM.

Although the total number of false transitions provides a metric to evaluate the performance of the HMM, it requires accurate knowledge of the motion interference instances, which are not precisely known. Thus, we relax the evaluation criteria such that a false positive is not accounted for if the person actually moves within a half a second time window with respect to the triggered time instant. Correspondingly, a false negative is not accounted for if motion interference is correctly identified by the HMM within a half a second time window. This metric is not only more realistic but it also allows one to account for uncertainty in motion instances. Under this metric, selecting $0.001 < P_{2|2} < 0.5$ and $0.5 < P_{1|1} < 0.999$ yields no false negatives and under 1% of false positives. If it is also required that there are no false positives, it can be achieved by selecting $0.001 < P_{2|2} < 0.2$ and $0.85 < P_{1|1} < 0.999$. To conclude, the HMM performance is not particularly sensitive to the changes in P.

D. Experiment 3

In realistic scenarios, the breathing rate can vary over time and therefore, it is important to investigate the accuracy of the system under varying breathing rates. In Fig. 8a, the

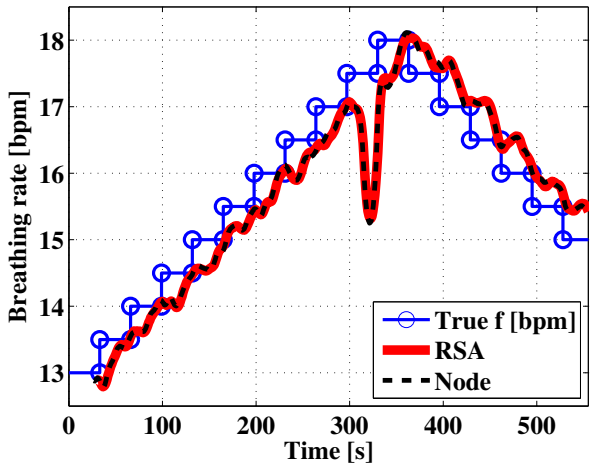

(a) Changing breathing rate w/o motion interference

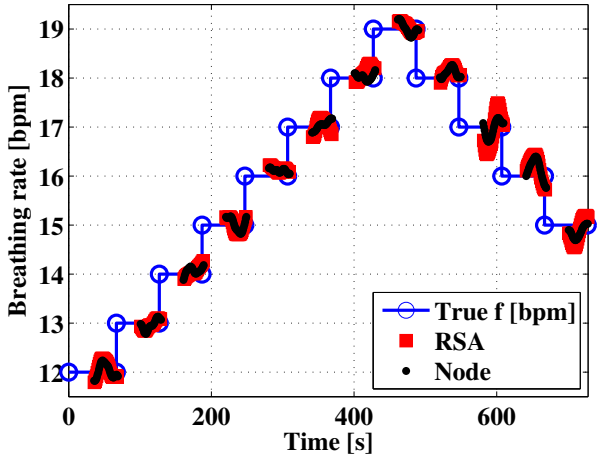

(b) Changing breathing rate with motion interference

Fig. 8: System performance when the breathing rate changes over time

TABLE III: Results of Experiment 3, test 1

		Node		RSA	
N [s]	K	ε_f [bpm]	$\varepsilon_{\%}$ [%]	ε_f [bpm]	$\varepsilon_{\%}$ [%]
15	542	0.2698	99.65	0.2582	100.0
30	528	0.2643	100.0	0.2456	100.0
45	513	0.3421	100.0	0.3322	100.0
60	499	0.4509	100.0	0.4418	100.0

TABLE IV: Results of Experiment 3, test 2

		Node		RSA	
N[s]	K	ε_f [bpm]	$\varepsilon_{\%}$ [%]	ε_f [bpm]	$\varepsilon_{\%}$ [%]
15	518	0.2712	99.80	0.2790	98.65
30	343	0.1174	100.00	0.1595	100.00
45	168	0.0833	100.00	0.0998	100.00
60	15	0.0548	100.00	0.0750	100.00

estimated breathing rate with respect to the true rate using the measurements of the first test of Experiment 3 is shown. On average, the estimated respiration rate follows the true breathing rate closely. However, the estimates contain a lag which is due to the window over which the PSD is calculated. A large window increases the lag of the estimates. On the other hand, a small window results that the estimates adapt to the changes rapidly but it can also result to inaccurate estimates as earlier demonstrated in Fig. 6c. $N = 94$ [samples] $\approx$ 30 [seconds] provides a good tradeoff between accuracy and adaptivity. Results of the test with different window lengths are summarized in Table III.

In Fig. 8a, the estimates of both systems deviate from the true breathing rate at time 320 s. This difference is not caused by inaccurate estimates; rather, a human-induced error during the experiment. At this time, there was external noise which distracted the person and resulted that the metronome was not heard clearly. As an outcome, the person lost track of the metronome and failed to breath at a constant rate. Evaluating the unprocessed measurements, it can be concluded that the estimated breathing rates are close to the person's breathing rate which erratically varied between 13 to 16 bpm as the person struggled to hear the metronome. Even though this incidence was unplanned, it demonstrates the systems capability to adapt even though the person's breathing rate changes drastically. This time window is omitted from the results of Table III.

The second test of Experiment 3 attempts to mimic real-world scenarios where the person's breathing rate varies over time in addition to possible posture changes. The estimated breathing rate with respect to the true rate is shown in Fig. 8b and the results are summarized in Table IV. The HMM is capable of identifying the motion interference instances correctly, enabling accurate breathing estimation during the experiment. With measurements of both systems, all estimates are valid when the window length is 30 s or larger. Moreover, using 30 s of data or more, the breathing rate can be estimated with an accuracy of $\varepsilon_f = 0.1595$ bpm or higher with both systems. For comparison, an end-tidal CO_2 meter, the gold standard breathing rate monitor used in hospitals [25], is accurate to ± 1 bpm.

E. Quantitative Comparison

In the following, we quantitatively compare the performance of the system under various conditions. We investigate the use of omni-directional antennas, a reduced number of frequency channels and lower sampling frequency. In addition, the effect of decimation to computational overhead is examined.

In order to evaluate the performance of the system under generalized conditions, we replace the directional antennas of the nodes with omni-directional antennas. The measurements are collected as in the second test of Experiment 3 where the posture and breathing rate is changed once per minute. In Fig. 9a, the estimated breathing rate with respect

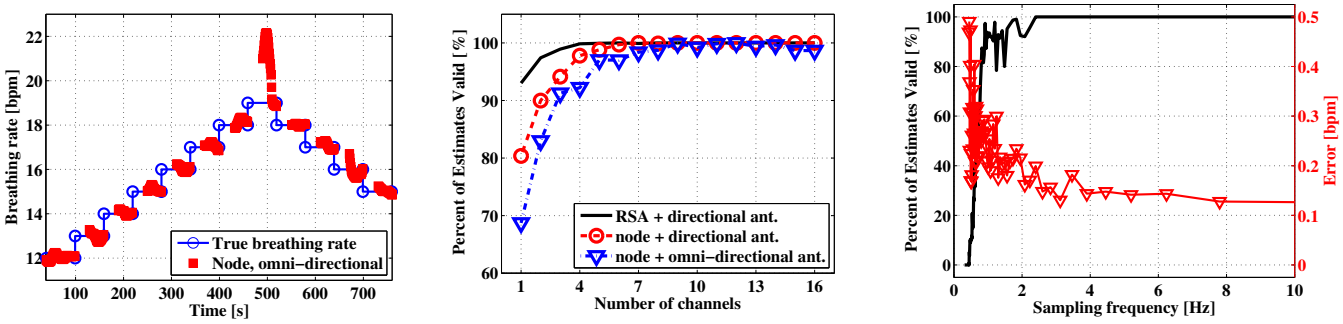

(a) Effect of omni-directional antennas (b) Effect of channel number C (c) Effect of sampling frequency f_s

Fig. 9: Performance of the system under various conditions

to the true rate is shown. On average, the respiration rate can be estimated with an accuracy that is comparable to the results obtained with the measurements of the RSA and node with directional antennas, since $\varepsilon_f = 0.1230$ bpm and $\varepsilon_{\%} = 95.27\%$. However, omni-directional antennas are more sensitive to the experimental setup since the sensitivity region of these antennas is not restricted in between the TX-RX pair. Thus, it is possible that the amplitude of the breathing affected multipath components is not large enough compared to the other multipath components impinging on the RX antenna to cause a measurable change in RSS. Due to this, breathing estimation fails in Fig. 9a at time (≈ 480 s).

The effect of used number of frequency channel to the accuracy of breathing estimation with different hardware configurations is shown in Fig. 9b. As can be concluded, the sensitivity order to the used channel number is: 1) node and omni-directional antenna; 2) node and directional antenna; 3) RSA and directional antenna. Using the measurements of a single channel and omni-directional antennas with the nodes, only 69% of the estimates are within ± 1 bpm of the true breathing rate. Respectively, the measurements of directional antennas and the node result to $\varepsilon_{\%} = 80\%$, whereas the RSA measurements yield $\varepsilon_{\%} = 93\%$. Thus, channel diversity not only enhances SNR of the noisy RSS measurements but it also decreases undesirable effects of multipath propagation and interference. To conclude, it is possible to estimate the breathing rate using a single frequency channel, however, the performance and applicability of the system can be drastically improved by using more channels.

In this paper, oversampling is exploited to increase quality of the RSS measurements. However, it is not always possible to probe the channel at such frequencies e.g. when more nodes are used to include spatial diversity to the measurements. Therefore, it is important to investigate the effect of sampling frequency on breathing estimation accuracy. In the analysis, we decrease the sampling rate of the original RSS measurements using

$$\hat{\boldsymbol{r}}(l) = \boldsymbol{r}(\Delta n),$$

where $\Delta = 1, 2, \cdots$. The results of breathing estimation using a lower sampling frequency along with $\varepsilon_{\%}$ is shown in Fig. 9c. The sampling rates above 4 Hz yields negligible effect on breathing estimation accuracy. However, the breathing rate estimation error becomes inversely proportional to sampling frequency in the case $f_s < 4$ Hz. Most notably, the number of valid breathing estimates decreases rapidly as the sampling frequency is reduced. Comparing the sampling frequencies and results with [4] ($f_s = 4.16$ Hz, $\varepsilon_f = 0.3$ bpm) and [6] ($f_s = 2.34$ Hz, $\varepsilon_f = 1.0$ bpm), we conclude that the achieved higher accuracy of the proposed system is due to the improved SNR. We exploit oversampling and filtering, low-jitter periodic communication, channel diversity, and directional antennas to increase SNR of the RSS measurements.

Decimation reduces the computational overhead significantly, since not only is the number of measurements lower (N/M) but also the number of FFT points can be reduced to achieve the same resolution. For example, the average computation times of breathing estimation, using decimation factors of $M = [1, 5, 10, 20]$ are $[0.893, 0.086, 0.045, 0.028]$ seconds on a standard laptop computer, a reduction of $[0.0\%, 90.4\%, 95.0\%, 96.9\%]$ in computation times. Therefore, especially when decimation is exploited, implementing an online algorithm for breathing estimation is very possible.

This paper addresses basic problems that are faced in breathing monitoring and additional work is required to enable practical applications. Important research questions include: to what extent will a person's movement be considered as motion interference so that breathing estimation is not possible? For example, will a small arm movement dominate the frequency content of the measurements? Is it possible that during such instances, some frequency channels are unaffected enabling breathing monitoring despite motion interference? Also, it should be studied how the person's size, age, gender, etc. affect breathing monitoring. For example, an infants chest movement is considerably smaller than for an adult and therefore, it is expected that for small children breathing monitoring is considerably harder.

VI. Conclusions

In this paper, we address respiration rate monitoring using low-cost commercial off-the-shelf transceivers. We propose a system composed of a single TX-RX pair, which significantly improves applicability of existing signal strength based breathing monitoring systems. Pre-filtering is exploited to increase SNR of the RSS measurements, channel diversity is used to increase the probability of breathing detection, and a motion interference detector is developed to identify time instances when breathing estimation is not possible. With the developed breathing monitoring system, we empirically demonstrate that using a single TX-RX pair, the respiratory rate of a person can be estimated with an accuracy comparable to the performance of a high-end spectrum analyzer for $3-4$ orders of magnitude less price. The proposed system does not require a sophisticated sensing technology, measurement equipment or complex system setup. In addition, the system can be battery powered enabling comprehensive application opportunities and use-case scenarios, which are either infeasible or impossible with other systems proposed to date.

Acknowledgment

This work is supported, in part, by Finnish Funding Agency for Technology and Innovation under the project WISM II. The work is also supported, in part, by the US National Science Foundation under Grant Nos. 0855261 and 1035565. The authors wish to thank Viktor Nässi for the help and guidance while preparing the experiments.

References

[1] A. F. Molisch, *Wireless Communications (Wiley - IEEE)*, 2nd ed. Wiley, 2010.

[2] H. Hashemi, "The Indoor Radio Propagation Channel," *Proc. IEEE*, vol. 11, no. 7, pp. 967–978, 1993.

[3] N. Patwari and J. Wilson, "RF sensor networks for device-free localization and tracking," *Proceedings of the IEEE*, vol. 98, no. 11, pp. 1961–1973, Nov. 2010.

[4] N. Patwari, J. Wilson, S. Ananthanarayanan P.R., S. Kasera, and D. Westenskow, "Monitoring breathing via signal strength in wireless networks," *Mobile Computing, IEEE Transactions on*, 2013, appeared online: 26 August 2013.

[5] F. Q. AL-Khalidi, R. Saatchi, D. Burke, H. Elphick, and S. Tan, "Respiration rate monitoring methods: a review," *Pediatric pulmonology*, vol. 46, no. 6, pp. 523–529, 2011.

[6] N. Patwari, L. Brewer, Q. Tate, O. Kaltiokallio, and M. Bocca, "Breathfinding: A wireless network that monitors and locates breathing in a home," *Selected Topics in Signal Processing, IEEE Journal of*, vol. 8, no. 1, pp. 30–42, Feb 2014.

[7] J. F. Fieselmann and C. M. Helms, "Respiratory rate predicts cardiopulmonary arrest for internal medicine inpatients," *Journal of general internal medicine*, vol. 8, no. 7, pp. 354–360, 1993.

[8] M. Folke, L. Cernerud, M. Ekström, and B. Hök, "Critical review of non-invasive respiratory monitoring in medical care," *Medical and Biological Engineering and Computing*, vol. 41, no. 4, pp. 377–383, 2003.

[9] Y. Chen, D. Misra, H. Wang, H.-R. Chuang, and E. Postow, "An x-band microwave life-detection system," *Biomedical Engineering, IEEE Transactions on*, vol. BME-33, no. 7, pp. 697–701, 1986.

[10] J. Salmi and A. Molisch, "Propagation parameter estimation, modeling and measurements for ultrawideband mimo radar," *Antennas and Propagation, IEEE Transactions on*, vol. 59, no. 11, pp. 4257–4267, 2011.

[11] N. Rivera, S. Venkatesh, C. Anderson, and R. Buehrer, "Multi-target estimation of heart and respiration rates using ultra wideband sensors," in *14th European Signal Processing Conference*, 2006.

[12] C. Li, J. Ling, J. Li, and J. Lin, "Accurate doppler radar noncontact vital sign detection using the relax algorithm," *Instrumentation and Measurement, IEEE Transactions on*, vol. 59, no. 3, pp. 687–695, 2010.

[13] "Kai Continuous: Non-Contact, Continuous Respiratory Rate Monitor," http://www.kaimedical.com.

[14] A. Droitcour, O. Boric-Lubecke, V. Lubecke, J. Lin, and G. Kovacs, "Range correlation and i/q performance benefits in single-chip silicon doppler radars for noncontact cardiopulmonary monitoring," *Microwave Theory and Techniques, IEEE Transactions on*, vol. 52, no. 3, pp. 838–848, 2004.

[15] A. V. Oppenheim, R. W. Schafer, and J. R. Buck, *Discrete-time signal processing*. Prentice Hall, 1999.

[16] P. Sebel, M. Stoddart, R. E. Waldhorn, C. Waldman, and P. Whitfield, *Respiration: The Breath of Life*. Torstar Books, 1985.

[17] J. F. Murray, *The Normal Lung: The Basis for Diagnosis and Treatment of Pulmonary Disease*, 2nd ed. W.B. Saunders Co., 1986.

[18] R. J. Bultitude, "Measurement, characterization, and modeling of indoor 800/900 MHz radio channels for digital communications," *IEEE Communications*, vol. 25, no. 6, pp. 5–12, 1987.

[19] J. A. Roberts and J. R. Abeysinghe, "A two-state Rician model for predicting indoor wireless communication performance," in *IEEE ICC*, vol. 1, June 1995, pp. 40–43.

[20] C. W. Therrien, *Discrete random signals and statistical signal processing*. Prentice Hall PTR, 1992.

[21] F. J. Massey and W. J. Dixon, *Introduction to Statistical Analysis,*. McGraw-Hill book company, 1969.

[22] "L-com's HG2409P high performance directional flat patch antenna," http://www.l-com.com.

[23] "Fundamentals of real-time spectrum analysis," http://www.tek.com.

[24] "Ieee 802.15.4 - 2006 standard," pp. 1–320, 2006.

[25] T. M. Cook, N. Woodall, J. Harper, and J. Benger, "Major complications of airway management in the {UK}: Results of the fourth national audit project of the Royal College of Anaesthetists and the Difficult Airway Society. Part 2: Intensive care and emergency departments," *British Journal of Anaesthesia*, vol. 106, no. 5, pp. 632–642, 2011.